J Solid State Electrochem (2009) 13:309–320
DOI 10.1007/s10008-008-0544-0

ORIGINAL PAPER

Mechanism of anodic oxidation of tungsten in neutral sulphate-fluoride solutions

Vassil Karastoyanov · Martin Bojinov

Received: 10 January 2008 / Accepted: 6 March 2008 / Published online: 12 April 2008

Abstract The anodic oxidation of tungsten has been studied in 1 M Na_2SO_4 solutions containing 0–0.25 M NaF. Steady-state currents measured in the passivation and passivity ranges increase significantly with increasing fluoride concentration, indicating enhanced dissolution of the oxide film. The electrochemical impedance response is dominated by the processes in the barrier layer and at its interface with the electrolyte. The presence of a pseudo-inductive loop in the impedance spectra at intermediate frequencies indicates point defect interaction during film growth and dissolution processes. A kinetic model including the recombination reaction between oppositely charged point defects at the film/solution interface as well as a kinetic scheme for tungsten dissolution through the film mediated by cation vacancies is proposed. It is found to reproduce satisfactorily the steady-state currents and the impedance spectra in the potential range 0.2–2 V. Such a model for the conduction mechanism in the barrier layer is believed to be an essential part of a modelling approach to the formation of a nanoporous overlayer on tungsten in fluoride-containing solutions.

Keywords Tungsten · Anodic oxide film · Point defect · Impedance spectroscopy · Kinetic model

Abbreviations

a	half-jump distance, cm
b_i	coefficients of the interfacial reactions (i=2,31), V^{-1}
C_b	capacitance of the barrier layer, F cm^{-2}
C_O	pseudo-capacitance due to modulation of film thickness, F cm^{-2}
D_O	diffusion coefficient of oxygen vacancies, cm^2 s^{-1}
D_M	diffusion coefficient of cation vacancies, cm^2 s^{-1}
E	applied potential, V
$\vec{E}$	electric field strength, V cm^{-1}
F	Faraday constant, 96485 C mol^{-1}
I	current density, A cm^{-2}
I_M	current density due to cation vacancies, A cm^{-2}
I_O	current density due to oxygen vacancies, A cm^{-2}
J_M	flux of tetravalent niobium cation vacancies, mol cm^{-2} s^{-1}
J_O	flux of oxygen vacancies, mol cm^{-2} s^{-1}
j	imaginary unit
k_i	rate constants of the interfacial reactions (i=2,31,32,4), mol cm^{-2} s^{-1}
k_d	rate constant of the film dissolution reaction, cm s^{-1}
k_M	constant defined in Eq. 18, A cm^{-2}
k_{WO3}	constant defined in Eq. 19, A cm^{-2}
L	thickness of the barrier layer, cm
$L_{F/S}$	width of the cation vacancy accumulation layer at the film/solution interface, cm
M	tungsten atom in the metal phase
$W_W^{V'}$	W(V) in a W(VI) position in the barrier film
W_W^{VI}	W(VI) in a W(VI) position in the barrier film
W_W^{VI*}	W(VI) in a W (VI)* position in the outermost cation layer of the film
O_O	oxygen position in the barrier film
$V_O^{\cdot\cdot}$	oxygen vacancy in the barrier film
$V_W^{6'}$	tungsten cation vacancy in the barrier film
S	capture cross-section for a positive defect, cm^2 C^{-1}
Z_M	impedance due to cation vacancies, Ω cm^2
$Z_{M,f}$	impedance due to transport of cation vacancies in the film, Ω cm^2

V. Karastoyanov · M. Bojinov (✉)
Department of Physical Chemistry,
University of Chemical Technology and Metallurgy,
Kl. Ohridski Blvd. 8,
1756 Sofia, Bulgaria
e-mail: martin@uctm.edu

$Z_{M,F/S}$ impedance due to cation vacancies at the film/solution interface, Ω cm^2
Z_O impedance due to oxygen vacancies, Ω cm^2
$Z_{O,f}$ impedance due to transport of oxygen vacancies in the film, Ω cm^2
q_n negative surface charge due to accumulation of cation vacancies, C cm^{-2}
α polarisability of the film/solution interface
α_i transfer coefficient ((i=2, 31)
β total number of cation positions per unit surface, mol cm^{-2}
γ_5 fraction of W(V) in W(VI) positions in the outermost layer of the film
γ_6 fraction of W(VI) in W(VI) positions in the outermost layer of the film
γ_6^* fraction of W(VI) in W(VI)* positions in the outermost layer of the film
ε dielectric constant of the film
ε_0 dielectric permittivity of vacuum, F cm^{-1}
ω angular frequency, rad s^{-1}

Introduction

Recently there have been numerous attempts to improve the performance of Pt-type electrocatalysts for methanol oxidation by dispersing them in large-surface-area nanocrystalline inorganic oxide matrices. Such a composite catalyst would ensure a homogeneous distribution of catalytic centers, as well as facilitate charge distribution, and overall stability [1, 2]. Tungsten oxide seems to promote electrochemical oxidation of methanol by interacting with Pt via hydrogen spillover or through the formation of highly conductive tungsten bronzes [3–9]. In addition, this oxide has been receiving considerable attention in recent years for its NO_x, CO, and H_2S gas sensing properties [10, 11] as well as for use in electrochromic [12–14], photochromic [15, 16] and transparent conducting electrode applications [17, 18].

Our interest is in developing a simple route of producing ordered nanoporous tungsten oxide structures based on anodisation. Anodisation of W to produce barrier-type oxides has been reported by numerous authors [19–41]. Film composition has been reported to be very close or practically identical to WO_3. The anodic film is a wide band-gap amorphous semiconductor (mobility gap, 2.8–3.1 eV). The donor concentration as estimated from Mott–Schottky analysis has been found to depend on film thickness either according to a power or an exponential law. Photoelectrochemical impedance and transient measurements point to a major role of the first atomic layer near the film/electrolyte interface in the kinetics of electron-hole recombination via surface states. In addition, film thickness vs time measurements have indicated that dissolution of the oxide plays an important role during film growth and the process of thickness increase is controlled by interfacial processes rather than conduction in the bulk oxide. The formation of ordered nanoporous anodic oxides on W has been reported very recently during oxidation in oxalic acid [42] and sulphate-fluoride electrolytes [43] at comparatively low voltages, whereas a possibility of fast growth of oxide nanotubes promoted by oxide breakdown in chloride or perchlorate electrolytes at higher voltages has been also demonstrated [44].

In the present paper, we report electrochemical measurements of the formation and properties of the anodic oxide on W in 1 M Na_2SO_4 containing 0–0.25 M NaF. Steady-state current vs potential curves and electrochemical impedance spectroscopic measurements have been employed to characterise the individual steps of the overall oxidation reactions that are detectable by electrochemical means. The impedance spectra as depending on potential and fluoride concentration have been quantitatively interpreted by an updated version of the surface charge approach [31, 32]. Several kinetic, transport and structural parameters characterising the conduction mechanism in the oxides have been estimated by quantitative comparison of the model to the experimental results. The parameter values as depending on fluoride concentration have been discussed with regard to their importance in the processes of subsequent formation of an ordered nanoporous overlayer at higher potentials.

Materials and methods

The working electrode material was pure W (99.9%, Goodfellow). Wire or disc-shaped cuts of that material were insulated with epoxy resin and inserted in PTFE holders to expose an area of 0.00785 cm^2 to the electrolyte. The working electrodes were mechanically abraded with emery paper up to grade 2400, rinsed with bidistilled water and dried by hot compressed air. The electrolytes were prepared from reagent grade Na_2SO_4 and NaF using bidistilled water. A conventional electrolytic cell featuring a large area Pt mesh counter electrode and a saturated calomel electrode (SCE) was employed. All the potentials in the paper are given vs this electrode.

The experiments were performed at room temperature (20±1 °C) in naturally aerated solutions (no effect of nitrogen purging on the results has been found in preliminary tests). The electrochemical measurements—steady state current vs potential curves and impedance spectra in the range 0.2–2.0 V vs SCE, have been carried out using an Autolab PGSTAT30+FRA, GPES and FRA2

software (EcoChemie). After a steady-state current was reached (criterion: variation of the current with time less than ±2% by magnitude), impedance spectra have been registered in the frequency range 20 mHz to 51 kHz at an alternating current (ac) amplitude of 15 mV (rms). The reproducibility of the impedance spectra was ±1% by impedance magnitude and ±2° by phase angle. The linearity of the impedance spectra has been checked by measuring spectra at ac amplitudes ranging from 5 to 20 mV, whereas causality was verified by a Kramers–Kronig compatibility test embedded in the measurement software. For the simulation and non-linear least squares fitting of impedance spectra, Origin 7.5 based routines were employed.

Results

Current vs potential curves

The current vs potential curves were measured in the potential range from 0.2 to 2 V to characterise both the active-to-passive transition and the passive range of W. Figure 1 shows current vs potential curves of W measured in 1 M Na_2SO_4+(0÷0.25 M) NaF. The active-to-passive transition is observed in the potential range 0.3–0.9 V and is the more pronounced, the higher is the NaF concentration. In other words, the passivation current density is larger at higher NaF concentrations, whereas the difference in magnitude between the critical passivation current density and the current density in the passive state is also somewhat smaller. This fact indicates that dissolution of W through the oxide is favoured by NaF addition to 1 M Na_2SO_4. On the other hand, there is no significant dependence of the passivation potential on NaF concentration, which probably means that the nature of the rate limiting steps of the overall reaction is not altered by NaF addition to the 1 M Na_2SO_4 electrolyte.

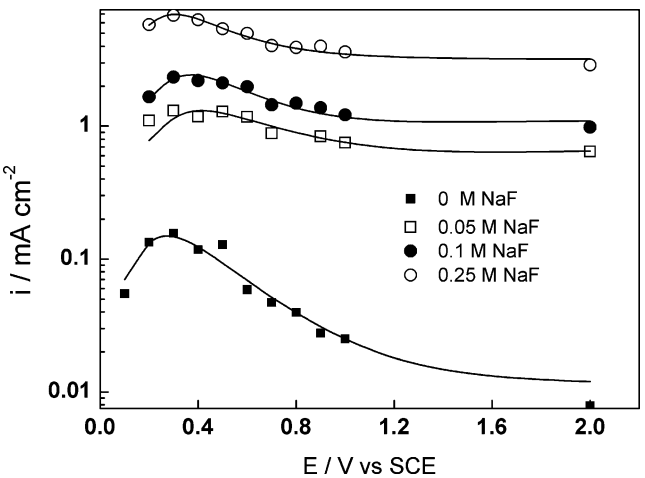

Fig. 1 Current vs potential curves of W in 1 M Na_2SO_4+0÷0.25 M NaF in the potential interval 0–2 V. *Points*—experimental values, *solid lines*—best-fit calculation according to the proposed model

In the passive range (above 1 V), the current density is only slightly dependent on potential, indicating that the chemical dissolution of the oxide is probably the rate controlling step of the overall oxidation process. The steady-state current in the passive state increases quasi-linearly with NaF concentration implying a first order of the film dissolution reaction with respect to NaF.

Impedance spectra

The impedance spectra for the W/WO_3/1 M Na_2SO_4 system in the passivation region (0.4–1.0 V) without NaF and with the addition of 0.25 M NaF are presented in Figs. 2 and 3. Qualitatively analogous spectra have been obtained in solutions containing 0.05 and 0.1 M NaF. Compilations of spectra at 2.0 V in all studied electrolytes are shown in Fig. 4 (1 M Na_2SO_4 and 1 M Na_2SO_4+0.05 M NaF) and Fig. 5 (1 M Na_2SO_4+0.1 and 0.25 M NaF).

The impedance magnitude at low frequencies $Z_{f\to 0}$ decreases significantly with increasing NaF concentration, in line with the increase in the current density (Fig. 1). On the other hand, at potentials above the active-to-passive transition $Z_{f\to 0}$ is found to increase with potential, as observed also by other authors in a range of solutions [30, 31, 38]. This trend most probably reflects the influence of the film thickness (which increases linearly with potential, as is well-known for oxide growth on valve metals) on the impedance magnitude [30, 31, 38].

The oxide film resistance and capacitance dominate the impedance response at high-frequencies. In the intermediate frequency range, a pseudo-inductive response becomes visible at potentials higher than 0.5 V, i.e. in general before the passivation peak, in analogy to earlier results with Nb in sulphate-fluoride electrolytes and Mo in phosphoric acid [32]. The appearance of such a feature has been earlier ascribed to relaxation phenomena due to the formation and time variation of a negative surface charge at the oxide film/solution interface [30, 31]. This part of impedance spectra can be described with a low frequency time constant, $\tau_{LF} = R_{sc}.L_{sc}$. The value of this time constant (or the inverse of the characteristic frequency of the inductive loop) decreases with increasing NaF concentration, which indicates an accelerating effect of F^- addition on the build-up of the surface charge in the transient regime. At the low-frequency end, a further capacitive response is detected. In the active-to-passive transition region, it is most probably due to the passivation reaction as it tends to turn to a positive direct current (dc) limit at potentials below the critical potential for passivation and to a negative dc limit at potentials above that value. In the passive region, the capacitive response at low frequencies can be ascribed to

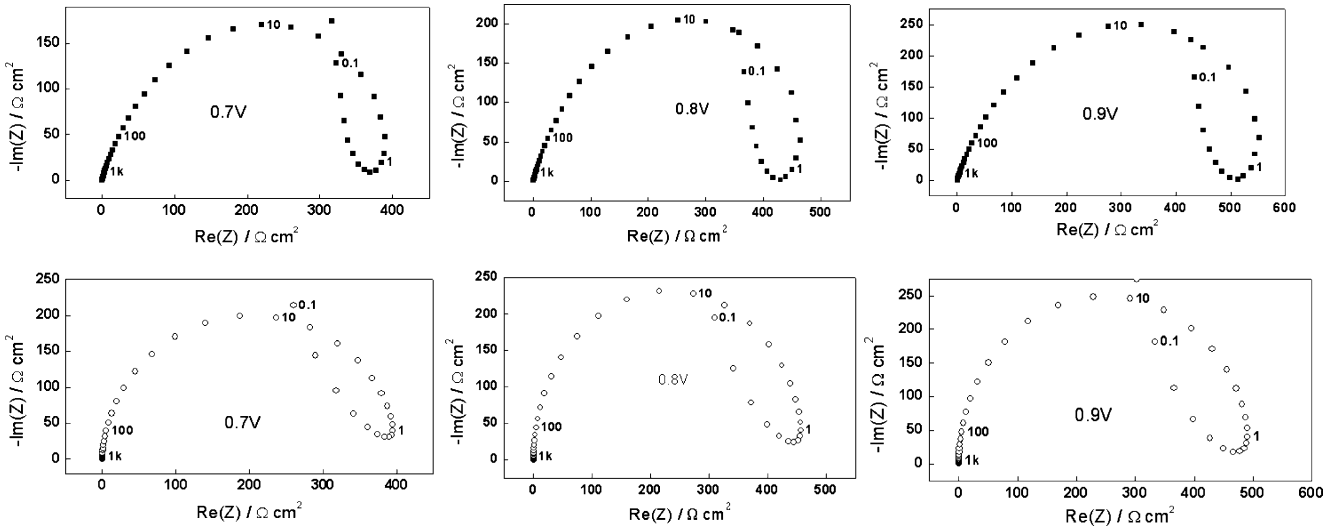

Fig. 2 Impedance spectra of W in 1 M Na $_2SO_4$. *Upper row*—experimental spectra, *lower row*—calculated spectra according to the proposed model. Parameter is frequency in Hertz

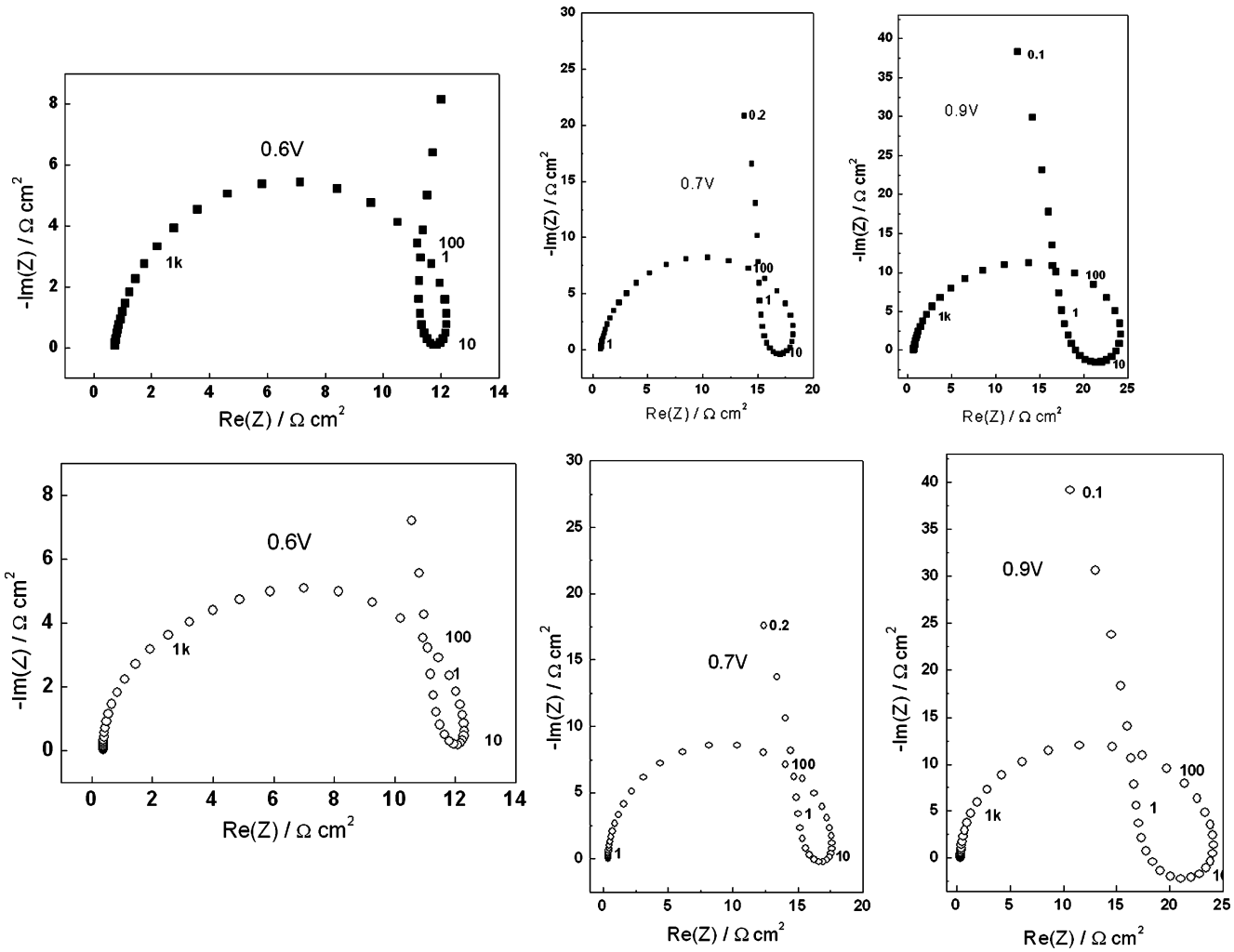

Fig. 3 Impedance spectra of W in 1 M Na $_2SO_4$+0.25 M NaF. *Closed symbols*—experimental spectra, *open symbols*—calculated spectra according to the proposed model. Parameter is frequency in Hertz

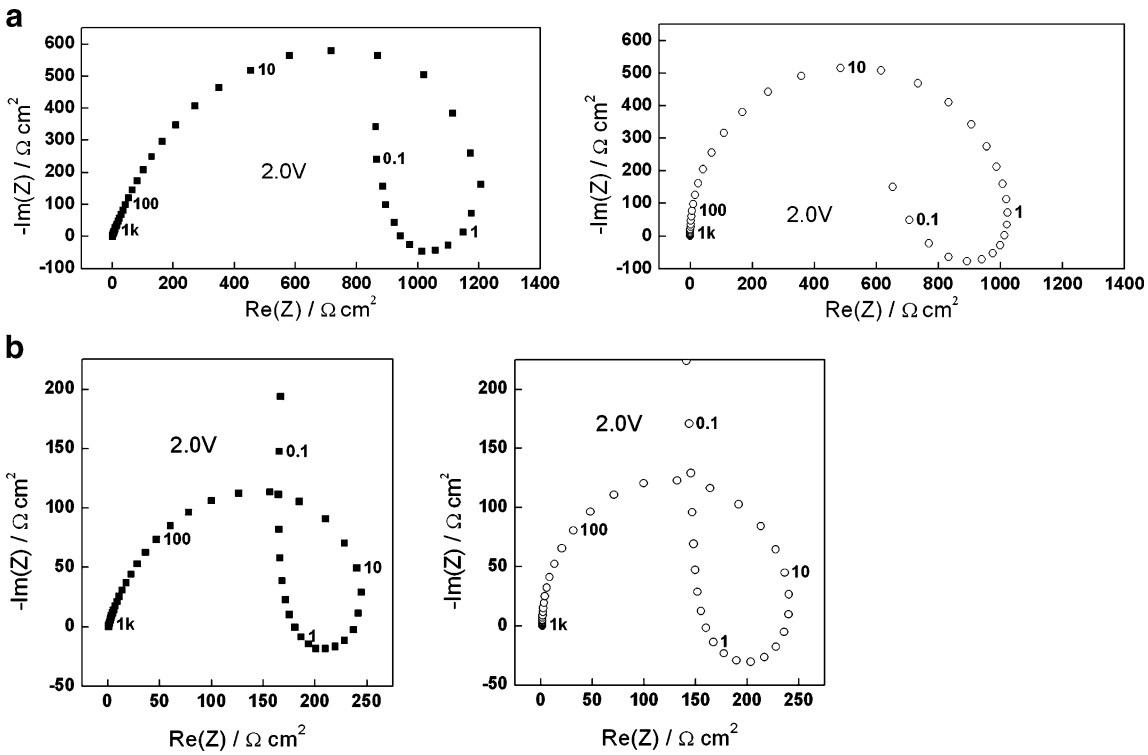

Fig. 4 Impedance spectra of W at 2.0 V in 1 M Na_2SO_4 (**a**) and 1 M Na_2SO_4+0.05 M NaF (**b**). *Closed symbols*—experimental spectra, *open symbols*—calculated spectra according to the proposed model. Parameter is frequency in Hertz

the relaxation of film thickness with ac modulation, as proposed by a range of authors [31, 32, 45, 46].

Summarising, the current vs potential curves and the ac impedance spectra in the passivation and passivity ranges of W in sulphate-fluoride solutions indicate a coupling between the dissolution of tungsten and the formation of a passivating oxide. To estimate in a quantitative fashion the kinetic and transport parameters pertinent to these two processes, an appropriate physico-chemical model has to be devised. The next section is devoted to the description of this model, which is based on an earlier approach to the passivation and passivity of Nb in sulphate-fluoride solutions [32].

Discussion

Chemical reactions in the W/WO_3/electrolyte system

The oxide of tungsten that forms at open circuit in an aqueous solution can be regarded as mixed-valency oxide [47] in which W(V) and W(VI) position coexist the cation sublattice, together with a certain concentration of W(VI) cation vacancies. A significant concentration of oxygen vacancies is assumed to exist in the anion sublattice as well. The growth of the passive film [29, 35] proceeds at the metal/film interface with oxidation of the metal and simultaneous generation of oxygen vacancies

$$m \rightarrow W_W^{VI} + 3V_O^{\bullet\bullet} + 6e_m \tag{1}$$

The oxygen vacancies are transported through the barrier film by high-field assisted migration and react with adsorbed water at the film/solution interface achieving film growth

$$3V_O^{\bullet\bullet} + 3H_2O \xrightarrow{k_4} 3O_O + 6H^+ \tag{2}$$

In order for the film thickness to be invariant with time in the steady state, a film dissolution reaction must be included

$$WO_z + 2zH^+ \xrightarrow{k_d} W^{6+} + zH_2O \tag{3}$$

In fluoride-containing electrolytes, fluoro- or oxyfluoro-complexes of W(VI) are probably formed, which is expected to increase the solubility or the dissolution rate of the film. Thus the steady-state current density governed by chemical dissolution of the oxide will increase with fluoride concentration, as observed experimentally. To account for the effect of fluoride on the rate of chemical dissolution of the oxide, reaction 3 could be rewritten as

$$WO_z + 2zH^+ + yF^- \xrightarrow{k_d} WO_zF_{y,aq}^{6-2z-y} + zH_2O$$

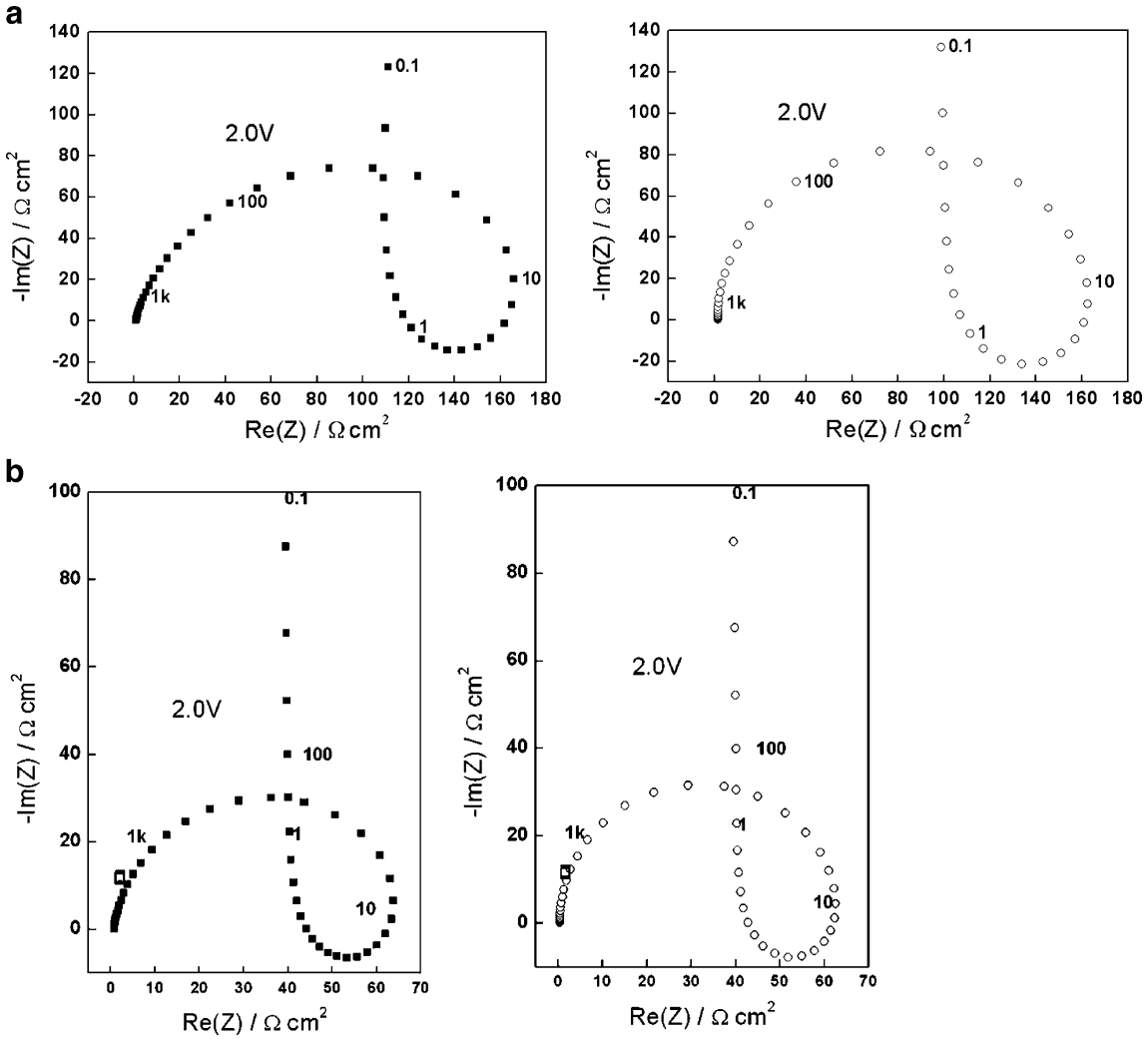

Fig. 5 Impedance spectra of W at 2.0 V in 1 M Na_2SO_4+0.1 M NaF (**a**) and 1 M Na_2SO_4+0.25 M NaF (**b**). *Closed symbols*—experimental spectra, *open symbols*—calculated spectra according to the proposed model. Parameter is frequency in Hertz

W(V) at the F/S interface undergoes either oxidative dissolution as W_{aq}^{6+} or transforms into a passivating W(VI)* species that dissolves isovalently:

$$W_W^{V'} \xrightarrow{k_2} W_{aq}^{6+} + e' + V_W^{6'} \tag{4}$$

$$\begin{aligned} W_W^{V'} &\xrightarrow{k_{31}} W_W^{VI*} + e' \\ W_W^{VI*} &\xrightarrow{k_{32}} W_{aq}^{6+} + V_W^{6'} \end{aligned} \tag{5}$$

The rates of both isovalent and oxidative dissolution of W(V) can be assumed to be increased by fluoride addition to the electrolyte as the final soluble products of these reactions will be also the fluoro- or oxyfluorocomplexes of W(VI). Therefore in general, reactions 4 and 5 can be written taking explicitly the effect of fluoride

$$W_W^{V'} + yF^- + zH_2O \xrightarrow{k_2} WO_zF_{y,aq}^{6-2z-y} + 2zH^+ + e' + V_W^{6'}$$

$$\begin{aligned} W_W^{V'} &\xrightarrow{k_{31}} W_W^{VI*} + e' \\ W_W^{VI*} + yF^- + zH_2O &\xrightarrow{k_{32}} WO_zF_{y,aq}^{6-2z-y} + V_W^{6'} + 2zH^+ \end{aligned}$$

Main equations

The tungsten cation vacancies, generated by reactions 4 and 5, are transported through the film via high-field

assisted migration or recombine with oxygen vacancies according to the reaction

$$V_{\mathrm{O}}^{\cdot\cdot} + \mathrm{V}_{\mathrm{W}}^{6'} \rightarrow \text{null} \tag{6}$$

The high-field migration equations for the transport of cation and anion vacancies are

$$J_o = -\frac{D_0}{2a} c_{\mathrm{O}}(L) e^{\frac{2Fa\vec{E}_0}{\mathrm{RT}}}, J_{\mathrm{M}} = c_{\mathrm{M}}(0)\frac{D_{\mathrm{M}}}{2a}\ e^{\frac{\chi Fa\vec{E}_0}{\mathrm{RT}}} \tag{7}$$

so that the total defect transport current density is $I = -2FJ_o + 6FJ_m$.

The instantaneous electric field strength in the metal /oxide/electrolyte system $\vec{E}_0$ is given by the sum of all the instantaneous potential drops in the system divided by film thickness [31]

$$\vec{E}_0 = \left(\phi_{\mathrm{M/F}} + \vec{E}L + \phi_{\mathrm{F/S}}\right)\Big/ L \tag{8}$$

where $\phi_{\mathrm{M/F}} = (1-\alpha)\mathrm{E} - \overrightarrow{\mathrm{E}}\mathrm{L}$, $\phi_{\mathrm{F/S}} = \mathrm{q_n L_{F/S}}/\varepsilon\varepsilon_0$, α is the polarisability of the film/solution interface, q_{n} is a negative surface charge due to accumulation of cation vacancies at the film/solution interface, $\vec{E}$ the field strength in the film bulk and $L_{\mathrm{F/S}}$ is the width of the cation vacancy accumulation layer [31]. Further, according to the Mixed-Conduction Model for oxide films [48], the potential drop at the metal/film interface does not depend on the applied potential. In other words, the reactions at this interface are not considered to be rate limiting. Rather, their rate is adjusted by the transport processes of point defects in the passive film.

The expressions of the instantaneous partial currents due to the transport of oxygen and cation vacancies acquire the form:

$$\begin{aligned} I_0 &= \tfrac{FD_0}{a} c_o(L) \quad \exp\left\{\tfrac{2Fa}{RTL}\left[(1-\alpha)E + \tfrac{q_n L_{\mathrm{L/S}}}{\varepsilon\varepsilon_0}\right]\right\}, \\ I_{\mathrm{M}} &= \tfrac{6FD_0}{2a} c_{\mathrm{M}}(0) \quad \exp\left\{\tfrac{6Fa}{RTL}\left[(1-\alpha)E + \tfrac{q_n L_{\mathrm{F/S}}}{\varepsilon\varepsilon_0}\right]\right\} \end{aligned} \tag{9}$$

In other words, the instantaneous fluxes of positive and negative defects are coupled via the recombination reaction which leads to the formation of a negative surface charge of cation vacancies at the film/solution interface in the transient regime. To evaluate the time dependence of the surface charge, the material balance of cation vacancies at this interface has to be calculated.

At the film/solution interface, cation vacancies are (1) generated with a current density $I_{\mathrm{M,F/S}}$, (2) transported via high-field migration with a current density I_{M} and (3) react with the oxygen vacancies according to the recombination reaction at a rate of $I_{\mathrm{O}} S q_{\mathrm{n}}$, where S is the cross-section of recombination. Then, for the time variation of the surface charge we obtain

$$\frac{\mathrm{d}q_n}{\mathrm{d}t} = I_{\mathrm{M,F/S}} - I_{\mathrm{M}} - I_{\mathrm{O}} S q_{\mathrm{n}} = I_O S\left(\frac{I_{\mathrm{M,F/S}} - I_{\mathrm{M}}}{I_{\mathrm{O}} S} - q_{\mathrm{n}}\right). \tag{10}$$

According to the dissolution scheme described by reactions 4 and 5, the current density due to cation vacancies at the film/solution interface is given by:

$$\frac{I_{\mathrm{M}}}{6F} = J_{\mathrm{M}}^{5'} = k_2\gamma_5 + k_{32}\gamma_6^* \tag{11}$$

γ_5 and γ_6^* being the fractions of the F/S interface occupied by W(V) and W(VI)*, referred to the cation sublattice only. It is assumed that the surface concentration of W(V) cation vacancies is considered as negligible with respect to γ_5 and γ_6^*. The material balances in the outermost cation layer are correspondingly:

$$\frac{\beta d\gamma_5}{dt} = \frac{I_M}{6F} - k_2\gamma_5 - k_{31}\gamma_5 \tag{12}$$

$$\frac{\beta \mathrm{d}\gamma_6^*}{\mathrm{d}t} = k_{31}\gamma_5 - k_{32}\gamma_6^* \tag{13}$$

Steady state solution and total current density

In the steady state equations 12 and 13 become

$$\frac{\overline{I}_{M,F/S}}{6F} - \overline{k}_2\overline{\gamma}_5 - \overline{k}_{31}\overline{\gamma}_5 = 0 \tag{14}$$

$$k_{32}\overline{\gamma}_5 - \overline{k}_{31}\overline{\gamma}_6^* = 0 \tag{15}$$

and obviously

$$\overline{\gamma}_5 + \overline{\gamma}_6^* + \overline{\gamma}_6 = 1 \tag{16}$$

$\overline{\gamma}_6$ being the surface fraction occupied by WO_3, i.e. regular W(VI) sites, at which the isovalent dissolution of the oxide (reaction 3) proceeds. Equations 11, 15 and 16 can be used to calculate $\overline{I}_{\mathrm{M,F/S}}$:

$$\overline{I}_{\mathrm{M,F/S}} = \frac{6Fk_{32}\left(\overline{k}_2 + \overline{k}_{31}\right)}{\overline{k}_{31} + \overline{k}_{32}}(1-\overline{\gamma}_6) = \overline{k}_{\mathrm{M}}(1-\overline{\gamma}_6) \tag{17}$$

$\overline{I}_{\mathrm{M}}$ is proposed to be proportional to the surface $(1-\overline{\gamma}_6)$ not occupied by regular W(VI), whereas $\overline{I}_{\mathrm{O}}$ is assumed to flow only on the fraction $\overline{\gamma}_6$.

$$\overline{I}_{\mathrm{O}} = 2Fk_d c_{\mathrm{H^+}}^n \overline{\gamma}_6 = 2Fk_{\mathrm{d}}^{'}\overline{\gamma}_6 = k_{\mathrm{WO_3}}\overline{\gamma}_6 \tag{18}$$

where n is the reaction order of the chemical dissolution reaction, Eq. 3 with respect to $\mathrm{H^+}$.

If we define γ_6 as a function of the reaction rates for the formation of W(V) and W(VI) centers

$$\overline{\gamma}_6 = \frac{k_{WO_3}}{\overline{k}_M + k_{WO_3}} \tag{19}$$

then

$$\overline{I}_M = \frac{\overline{k}_M^2}{\overline{k}_M + k_{WO_3}} \tag{20}$$

$$\overline{I}_O = \frac{\overline{k}_{WO_3}^2}{\overline{k}_M + k_{WO_3}} \tag{21}$$

Small amplitude ac solution

From the assumption that currents transported by oxygen and cation vacancies are additive, and taking into account the electronic properties of the oxide, the impedance of the system can be defined as the parallel combination of the impedance due to generation and transport of cation vacancies (Z_M), the impedance due to transport and consumption pf oxygen vacancies (Z_O) and the capacitance of the barrier film C:

$$Z = R_{el} + \left[j\omega C + \frac{1}{Z_O} + \frac{1}{Z_M} \right]^{-1} \tag{22}$$

where R_{el} is the electrolyte resistance. The film capacitance is defined as

$$C^{-1} = \frac{(1-\alpha)}{\varepsilon\varepsilon_0 \vec{E}} \overline{E} \tag{23}$$

Impedance due to transport and consumption of oxygen vacancies

For a small amplitude sinewave perturbation around a steady-state equation (Eq. 10) transforms into:

$$\widetilde{q}_n = \frac{\overline{I}_0 S\alpha \widetilde{E} \frac{\varepsilon\varepsilon_0}{L_{F/S}}}{j\omega + I_0 S}. \tag{24}$$

where $\widetilde{x}$ indicates the complex amplitude of a variable x. The migration current of oxygen vacancies in such conditions is given by

$$\widetilde{I}_o = \frac{2\overline{I}_0 B}{\overline{L}} \left[(1-\alpha)\widetilde{E} + \widetilde{q}_n \frac{L_{L/S}}{\varepsilon\varepsilon_0} \right], B = \frac{2Fa}{RT} \tag{25}$$

Solving 24 and 25 simultaneously, we obtain for the impedance of transport of oxygen vacancies

$$Z_{O,f}^{-1} = \frac{\Delta I_0}{\Delta E} = \frac{2\overline{I}_0 B}{L} \left[(1-\alpha) + \frac{I_0 S\alpha}{j\omega + I_0 S} \right] \tag{26}$$

To account for the capacitive behaviour observed in the impedance spectra at low frequencies, the ac modulation of the film thickness has to be taken into account. The expression for the ac current density due to that phenomenon has the form

$$\widetilde{I} = \frac{(1-\alpha)}{\lambda \vec{E}} \frac{V_m}{6F} j\omega \widetilde{E}, \tag{27}$$

which corresponds to a pseudo-capacitance in series with the impedance due to transport of oxygen vacancies, $\lambda = \frac{\overline{I}_O}{\overline{I}_O + \overline{I}_M}$ being the current efficiency for film formation:

$$C_0 = \left(\overline{I}_O + \overline{I}_M\right) \frac{(1-\alpha)}{\overline{I}_O \vec{E}} \frac{V_m}{6F} \tag{28}$$

The total impedance due to oxygen vacancies is then expressed as

$$Z_O = Z_{O,f} + \frac{1}{j\omega C_0} \tag{29}$$

Impedance due to generation and transport of cation vacancies

The faradaic impedance due to the generation of cation vacancies at the F/S interface is derived from Eqs. 11,12 and 13.

$$Z_{M,F/S}^{-1} = 6F \left[\widetilde{k}_2 \overline{\gamma}_5 + \overline{k}_2 \widetilde{\gamma}_5 + k_{32} \widetilde{\gamma}_6^* \right] \tag{30}$$

$$\begin{aligned} j\omega\beta\widetilde{\gamma}_5 &= \frac{Z_{M,F/S}^{-1}}{6F} - \widetilde{k}_2 \widetilde{\gamma}_5 - \widetilde{k}_2 \overline{\gamma}_5 - \widetilde{k}_{31} \overline{\gamma}_5 - \overline{k}_{31} \widetilde{\gamma}_5 \\ j\omega\beta\widetilde{\gamma}_6^* &= \widetilde{k}_{31} \overline{\gamma}_5 - \overline{k}_{31} \widetilde{\gamma}_5 - k_{32} \widetilde{\gamma}_6^* \end{aligned} \tag{31}$$

$$\widetilde{\gamma}_6^* = \frac{\overline{k}_{31} \widetilde{\gamma}_5 + \widetilde{k}_{31} \overline{\gamma}_5}{\beta j\omega + k_{32}} \tag{32}$$

$$\widetilde{\gamma}_5 = \frac{Z_{\mathrm{M,F/S}}^{-1}}{6F\left(\beta j\omega + \overline{k}_2 + \overline{k}_{31}\right)} - \frac{\overline{\gamma}_5\left(\widetilde{k}_2 + \widetilde{k}_{31}\right)}{\left(\beta j\omega + \overline{k}_2 + \overline{k}_{31}\right)} \tag{33}$$

$$Z_{\mathrm{M,F/S}} = 6Fb_2\overline{k}_2\overline{\gamma}_5\left[1 + \frac{b_{31}\overline{k}_{31}\left(\overline{k}_2 - \overline{k}_{31}\right)}{\left(1 + j\left(\frac{\omega\beta\overline{k}_2 b_2}{b_2 k_{32}\overline{k}_2 + b_{31}\overline{k}_{31}^2}\right)\right)\left(b_2\overline{k}_2 k_{32} + b_{31}\overline{k}_{31}^2 + \overline{k}_{31}\overline{k}_2(b_2 - b_{31})\right)}\right] \tag{34}$$

The impedance of the transport of cation vacancies is written in complete analogy to Eq. 26 as

$$Z_{\mathrm{M,f}}^{-1} = \frac{\Delta I_{\mathrm{M}}}{\Delta E} = \frac{6\overline{I}_{\mathrm{M}}B}{L}\left[(1-\alpha) + \frac{I_0 S\alpha}{j\omega + I_0 S}\right] \tag{35}$$

The total impedance due to generation and transport of cation vacancies, Z_{M}, is then given by:

$$Z_{\mathrm{M}} = Z_{\mathrm{M,f}} + Z_{\mathrm{M,F/S}} \tag{36}$$

Finally, the total impedance is calculated using Eqs. 22, 23, 29 and 36.

Comparison with the experimental results

To obtain quantitative estimates of the kinetic and transport parameters of the model via comparison with experimental data, the following two-step calculation procedure was adopted. First, the total current density vs potential curves have been fitted to the sum of Eqs. 20–21 with k_2^0, b_2, k_{31}^0, b_{31}, k_{32} and $k_{\mathrm{d}}^{'}$ as adjustable parameters. Second, keeping these values constant, the impedance spectra at potentials from 0.4 to 5 V have been fitted to the sum of Eqs. 22, 23, 29 and 36, using $\vec{E}$, α, a, S, β as adjustable parameters assuming a dielectric constant of 54 and a molar volume of 31 for the oxide phase of the passive film.

The current vs potential curves calculated by this best-fit procedure are shown in Fig. 1 with solid lines, whereas the calculated spectra for each solution at a range of potentials are presented with open symbols in Figs. 2, 3, 4 and 5. The estimated values of the rate constants k_2^0, k_{31}^0, k_{32} and $k_{\mathrm{d}}^{'}$ as depending on the NaF concentration are shown in Fig. 6, whereas the remaining parameters are collected in Table 1.

A satisfactory agreement for both the magnitude and the frequency distribution of the impedance is obtained in the whole potential range, indicating the validity of the proposed approach. The main discrepancies lie around the fact that at certain potentials the exact diameters of the two high-frequency loops are not matched with sufficient accuracy. While a better match could be gained by allowing some of the above parameters to vary with potential during the fit, this was not considered worthwhile due to the already large number of parameters involved in the calculation. It is encouraging that the whole set of data in a large potential range and in four solutions is reproduced with a rather homogeneous set of parameters (Table 1 and Fig. 6). The part of the potential consumed at the film/solution interface α, the exponential coefficients b_2 and b_{31} are independent on potential within the calculational error (Table 1), preserving values typical for film covered electrodes (the corresponding transfer coefficients α_2 and α_{31} are ca. 0.3–0.35). The values of the field strength are also well within the limits of the high-field approximation and do not exhibit any meaningful dependence on NaF concentration. This probably means that the transport properties of the oxide bulk are not altered significantly by NaF addition to the electrolyte, the effect of fluoride being restricted to the outermost layer of the film in contact with the solution.

The main effect of NaF addition is on two groups of parameters—on one hand, the rate constants k_2^0, k_{31}^0, k_{32}, $k_{\mathrm{d}}^{'}$ and the maximum surface concentration of W(VI)* sites β (characterising the processes of oxidation at the film/solution interface and generation of cation vacancies, as

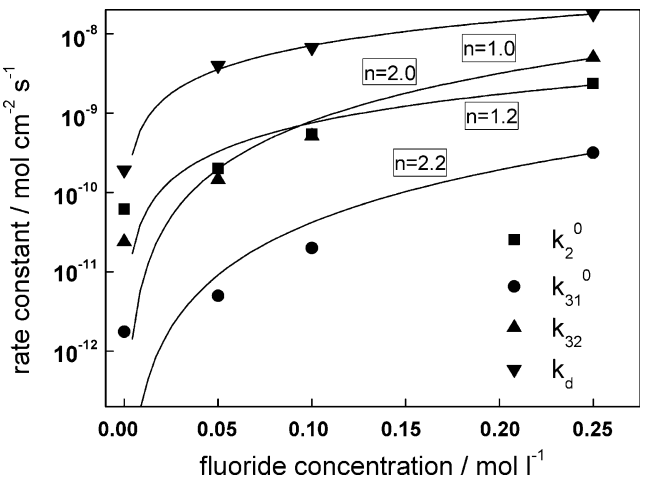

Fig. 6 Dependences of the standard rate constants at the film/electrolyte interface on NaF concentration

Table 1 Kinetic and transport parameters depending on NaF concentration

Parameter	1 M Na_2SO_4	1 M Na_2SO_4+0.05 M NaF	1 M Na_2SO_4+0.1 M NaF	1 M Na_2SO_4+0.25 M NaF
b_2/V^{-1}	11.4	10.6	10.6	10.5
b_{31}/V^{-1}	13.0	14.0	13.0	14.0
β/nmol cm^{-2}	0.10	0.48	0.2	0.46
a/nm	0.21	0.19	0.2	0.17
$\vec{E}$/MV cm^{-1}	2.7	5.3	2.5	4.2
α	0.39	0.39	0.39	0.39
S/mC^{-1} cm^2	11.58	18.0	8.27	12.0

well as the chemical dissolution of the film) and on the other, the half-jump distance a and the capture cross-section of recombination of cation and anion vacancies at the film/solution interface, S. The apparent reaction orders of the steps k_2^0, k_{31}^0, k_{32}, k_d' with respect to NaF concentration are given in the inserts of Fig. 6 and range between 1.0 and 2.2. Thus these reaction rate constants can be tentatively written as $k_2^0 = k_2^{00} c_{F^-}^{1.2}, k_{31}^0 = k_{31}^{00} c_{F^-}^{2.2}, k_{32} = k_{32}^{00} c_{F^-}^{2.0}, k_d' = k_d^0 c_{F^-}^{1.0}$.

Figure 7 shows the dependences of the surface fractions of the three tungsten species – W(V), W(VI)* and W(VI) on the applied potential for the anodic oxidation in the three fluoride-containing electrolytes. At potentials higher than 0.8 V, the surface fraction of W(V), $\overline{\gamma}_5$, is practically zero, and the surface is divided between W(VI)* and W(VI) species. In other words, in the passivity range the rate limiting steps of the overall reaction are the k_{32} and k_d steps, the rates of which are potential independent according to the proposed model. Thus the anodic oxidation is controlled by the rates of chemical dissolution reactions.

In a parallel study [49], the effect of pH in the range from 0 to 5 on the anodic oxidation of W in 1 M SO_4^{2-}+0.2 M F^- has been studied and the applicability of the model proposed in the present study has been confirmed. The estimated values of the rate constants k_2^0, k_{31}^0, k_{32} and k_d' as depending on pH at constant NaF concentration are shown in Fig. 8. The apparent reaction orders of the individual kinetic steps with respect to pH range between 0.4 and 0.5 (for k_2^0, k_{31}^0) and 0.1 and 0.2 (for k_{32}, k_d'). Thus the orders with respect to pH are smaller than those with respect to fluoride estimated in the present work. In other words, the effect of pH on reaction kinetics is of secondary importance in comparison to the effect of fluoride.

The maximum surface concentration of W(VI)* sites β seems to increase with NaF concentration indicating an increased defectiveness of the outermost layer of oxide in the presence of NaF. The same could be noticed for the maximum surface concentration of cation vacancies, as the capture cross-section of recombination can be related to such a parameter by the equation $S = (6F\beta_M)^{-1}$. The values of β_M calculated from the S values collected in Table 1 are of the order of 0.11 to 0.25 nmol cm^{-2}, i.e. they are rather close to the values of β. This can be taken as a

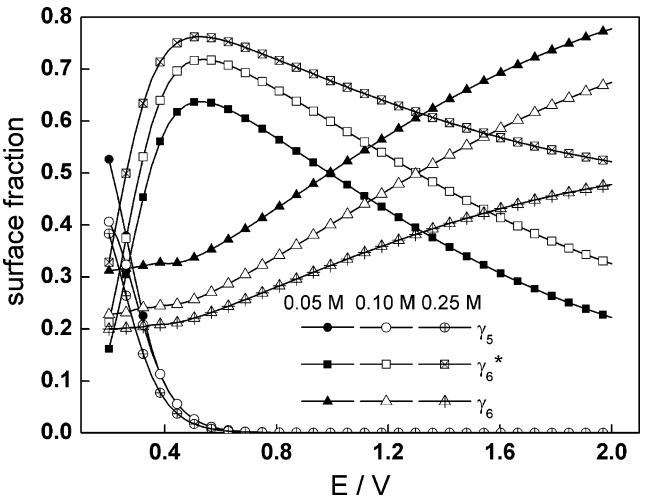

Fig. 7 Dependences of the surface fractions of W(V), W(VI)* and W(VI) on the applied potential for W in 1 M Na $_2SO_4$+0.05, 0.1 and 0.25 M NaF calculated by using the rate constants and exponential coefficients estimated from the model

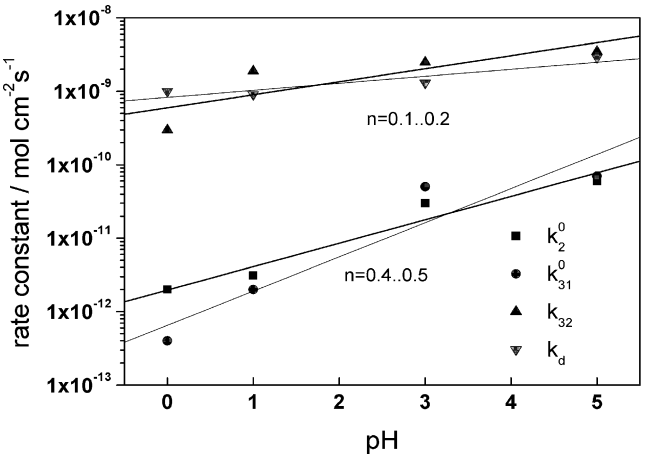

Fig. 8 Rate constants of the reactions of tungsten oxidation/dissolution at the oxide/electrolyte interface as depending on the pH of the 1 M SO_4^{2-}+0.1 F^- solution

further proof that the cation vacancies are generated by the reaction sequence 4–5 involving W(V) and W(VI)* sites.

Conclusions

The following conclusions can be drawn from the results obtained in the present work:

- The active-to-passive transition of W in 1 M Na_2SO_4 is the more prominent, the higher the addition of NaF to the electrolyte. This fact can be tentatively related to the increased production of cation vacancies by an increasingly non-stoichiometric outermost layer of the oxide film. The reaction steps of W(V) oxidation to W (VI)* and its subsequent isovalent dissolution have orders with respect to NaF that are close to unity indicating a strong accelerating effect of NaF on these two steps.
- In all studied electrolytes, the current density for W in the passive state is only slightly dependent on potential, indicating that the chemical dissolution of the oxide is probably the rate controlling step of the overall oxidation process in this region. The steady-state current increases quasi-linearly with NaF concentration implying a first order of the film dissolution reaction with respect to NaF, which has been predicted also by the calculations on the basis of the proposed model.
- The qualitative shape of impedance spectra is not affected by fluoride addition. The impedance magnitude at low frequencies decreases with increasing fluoride concentration in accordance to the concentration dependence of the steady state current density. The increase of the impedance magnitude at low frequencies with potential can be explained by the effect of increasing film thickness.
- A quantitative kinetic model involving processes at the film/solution interface and in the film bulk and also dissolution of tungsten through the oxide and oxide growth/dissolution as parallel reaction paths has been found to reproduce quantitatively the steady-state current vs potential curves and the impedance spectra in a wide range of potentials and solution compositions. The pseudo-inductive feature at intermediate frequencies is explained by the interaction between two current carriers of opposite sign, which accelerates the transport of the major current carrier in the transient regime.
- The main kinetic parameters of the model have been estimated and on the basis of their values hypotheses on the effect of NaF addition on the respective rates of the processes of oxide film growth and tungsten dissolution through the forming oxide have been proposed. The main effect of electrolyte composition is on the cross-section of recombination of current carriers at the film/solution interface, which can be tentatively ascribed to the influence of adsorbed fluoride ions on the defect structure of the outermost layer of the anodic film.

Further work is in progress to clarify the effect of pH at constant fluoride concentration on the passivation and passivity of tungsten in sulphate solutions.

Acknowledgement The funding of this work by the National Science Fund, Bulgarian Ministry of Education and Science, under contract ВУХ-307/2007 is gratefully acknowledged.

References

1. Hamnett A (1999) Interfacial electrochemistry—theory, experiment and applications, chap. 47. Marcel Dekker, New York, pp 871–873
2. Barczuk PJ, Tsuchiya H, Macak JM, Schmuki P, Szymanska D, Makowski O, Miecznikowski K, Kulesza PJ (2006) Electrochem Solid State Lett 9:E13
3. Kulesza PJ, Faulkner LR (1989) J Electroanal Chem 259:81
4. Shen PK, Tseung ACC (1994) J Electrochem Soc 141:3082
5. Shukla AK, Ravikumar MK, Arico AS, Candiano G, Antonucci V, Giordano N, Hamnett A (1995) J Appl Electrochem 25:528
6. Gotz M, Wendt H (1998) Electrochim Acta 43:3637
7. Kulesza PJ, Grzybowska B, Malik MA, Chojak M, Miecznikowski K (2001) J. Electroanal Chem 512:110
8. Yang LX, Bock C, MacDougall B, Park J (2004) J Appl Electrochem 34:427
9. Shim J, Lee CR, Lee HK, Lee JS, Cairns EJ (2001) J Power Sources 102:172
10. Kawasaki H, Namba J, Iwatsuji K, Suda Y, Wada K, Ebihara K, Ohshima T (2002) Appl Surf Sci 41:547
11. Gopel W, Schierbaum KD (1995) Sens Actuators B 26–27:1
12. Badilescu S, Ashrit PV (2003) Solid State Ionics 158:187
13. Granqvist CG (1999) Electrochim Acta 44:3005
14. Lee SH, Cheong HM, Zhang JG, Mascarenhas A, Benson DK, Deb SK (1999) Appl Phys Lett 74:242
15. Sun M, Xu N, Cao YW, Yao JN, Wang EG (2000) J Mater Res 15:927
16. Gavrilyuk AI (1999) Electrochim Acta 44:3027
17. Coutts TJ, Li X, Cessert TA (1990) IEEE Electron Lett 26:660
18. Stierna B, Granqvist CG (1991) Appl Opt 29:117
19. Nenov IP, Ikonopisov SM (1976) Compt Rend Bulg Acad Sci 29:39
20. Ord JL, Clayton JC, Brudzewski K (1978) J Electrochem Soc 125:908
21. Reichman B, Bard AJ (1979) J Electrochem Soc 126:583
22. DiQuarto F, DiPaola A, Sunseri C (1980) J Electrochem Soc 127:1016
23. DiQuarto F, DiPaola A, Sunseri C (1981) Electrochim Acta 26:1177
24. DiQuarto F, Russo G, Sunseri C, DiPaola A (1982) J Chem Soc Faraday Trans 1 78:3433
25. Hefny MM, El-Basiouny MS, Mogoda AS (1983) Corrosion 39:266
26. Goossens A, Macdonald DD (1993) Electrochim Acta 38:1965
27. Goossens A, Macdonald DD (1993) J Electroanal Chem 352:68

28. Biaggio SR, Rocha Filho RC, Vilche JR, Varela FE, Gassa LM (1994) J Braz Chem Soc 5:123
29. Sikora E, Sikora J, Macdonald DD (1996) Electrochim Acta 41:783
30. Biaggio SR, Rocha Filho RC, Vilche JR, Varela FE, Gassa LM (1997) Electrochim Acta 42:1751
31. Bojinov M (1997) Electrochim Acta 42:3489
32. Bojinov M, Cattarin S, Musiani M, Tribollet B (2003) Electrochim Acta 48:4107
33. Shimizu K, Brown GM, Habazaki H, Kobayashi K, Skeldon P, Thompson GE, Wood GC (1998) Corros Sci 40:1238
34. Macdonald DD, Sikora E, Sikora J (1998) Electrochim Acta 43:2851
35. Sikora J, Sikora E, Macdonald DD (2000) Electrochim Acta 45:1875
36. Anik M, Osseo–Asare K (2002) J Electrochem Soc 149:B224
37. Anik M (2002) Turk J Chem 26:915
38. Metikos-Hukovic M, Grubac Z (2003) J Electroanal Chem 556:167
39. Vergé MG, Olsson COA, Landolt D (2004) Corros Sci 46:2583
40. Olsson COA, Vergé MG, Landolt D (2004) J Electrochem Soc 151:B652
41. Anik M (2006) Corros Sci 48:4158
42. Varghese OK, Mor GK, Grimes CA (2003) J Mater Res 18:2296
43. Tsuchiya H, Macak JM, Sieber I, Taveira L, Ghicov A, Sirotna K, Schmuki P (2005) Electrochem Commun 7:295
44. Hahn R, Macak JM, Schmuki P (2007) Electrochem Commun 9:947
45. De Wit HJ, Wijenberg C, Crevecoeur C (1979) J Electrochem Soc 126:779
46. Young L, Yang TM, Backhouse C (1995) J Electrochem Soc 142:3479
47. Lim G, Lee JH, Son JW, Lee HW, Kim J (2006) J Electrochem Soc 153:B169
48. Bojinov M, Fabricius G, Laitinen T, Mäkelä K, Saario T, Sundholm G (2000) Electrochim Acta 45:2029
49. Karastoyanov V, Bojinov M (2008) Bulg Chem Comm (in press)